Bulletin of Geophysics and Oceanography Vol. XX, n. X, pp. XXX-XXX; Xxxxxx 20XX
DOI 10.4430/bgo00470

The physics of seismic propagation in aquifers partially saturated with H_2. Comparison with the cases of CO_2 and CH_4

D. Gei, J.M. Carcione and S. Picotti

National Institute of Oceanography and Applied Geophysics – OGS, Trieste, Italy

(Received: 17 May 2024; accepted: 21 July 2024; published online: 10 October 2024)

ABSTRACT This study presents a methodology to model the acoustic properties of a siliciclastic rock partially saturated with hydrogen (H_2), carbon dioxide (CO_2) and methane (CH_4). The gas properties are obtained with the Peng-Robinson equation of state, and pressure-temperature conditions, based on linear basin modelling with a constant geothermal gradient, are taken into consideration. The dry-rock bulk and shear moduli are obtained with the Krief model, while the Athy equation is used to calculate porosity as a function of depth. Mesoscopic attenuation and velocity dispersion due to fluid effects are quantified using the Johnson model. The viscoelastic Cole-Cole model is used to describe the velocities and attenuation predicted by the Johnson model when synthetic seismograms, with an equivalent viscoelastic rheology, are to be calculated. In this case, the P-wave velocity is calculated as a function of gas saturation using the Gassmann equation and an effective fluid modulus based on the Brie equation. This method can be used for feasibility studies on the geological storage of H_2 and CO_2 in aquifers and depleted CH_4 fields.

Key words: H_2, acoustics, geological storage, seismic monitoring.

1. Introduction

Hydrogen (H_2) is currently gaining importance as a future low-carbon energy carrier. The role that H_2 can play as a clean energy solution for the decarbonisation of transport, electricity, heating, and fuel-intensive industries to reduce greenhouse gas emissions on a large scale is increasingly recognised (Miocic *et al*., 2022). The use of green H_2 has seen unprecedented economic and political momentum, and the large volumes required to meet future demands would require new storage facilities. To advance new H_2 technologies, accurate information on acoustic properties is important if underground storage and monitoring is to be implemented. Depleted reservoirs and saline aquifers have the potential to provide the required storage volume (e.g. Carcione *et al*., 2020). The possibility of storing H_2 in such reservoirs and, then, withdrawing it repeatedly to cover fluctuations in energy demand, is currently being investigated (e.g. Barison *et al*., 2023; Mattera *et al*., 2023). Gas disposal should take place at supercritical pressures in order to avoid the presence of the gas phase and to make the best possible use of the storage volume.

The effects of pore pressure on the frame of the host rock and the contrast between the acoustic properties of the brine and those of H_2 are the most important factors for detecting and monitoring the presence of H_2 (e.g. Carcione *et al*., 2023). The variations may indicate that seismic methods can be used to detect and monitor the presence and flow of H_2 in the subsurface. Initially, the fluid properties are defined as a function of pressure and temperature, where the

acoustic gas properties are obtained from the van der Waals (VDW) and Peng-Robinson (PR) equations of state (EoSs). The possibility that H_2 may dissolve in the brine is not considered, as the solubility of this gas is negligible (Chabab *et al*., 2020) [0.0012 g of gas per kilogram of water at 60 °C and 0.1 MPa, compared to 0.5 for carbon dioxide (CO_2)]. Carcione *et al*. (2006) show that the amount of dissolved CO_2 is very small (see their Fig. 5), and the same is expected for H_2, mainly because of its low solubility.

The dry-rock moduli are obtained with the Krief model and the effects of pore pressure changes are considered through the porosity calculated with the Athy equation. The wet-rock moduli and seismic velocity are obtained using the Gassmann equation and the Johnson model, which also provides the attenuation factor.

Viscosity is essential for the quantification of seismic attenuation in the Johnson model. The viscosities of H_2, CO_2, and methane (CH_4) are determined as a function of pressure and temperature from the Lohrenz-Bray-Clark (LBC) theory (Lohrenz *et al*., 1964). Brine bulk modulus, density, and viscosity are calculated using empirical formulae proposed by Batzle and Wang (1992).

Seismic numerical modelling is often based on dynamic equations of wave propagation solved in the time domain, with viscoelasticity to model wave attenuation based on Cole-Cole or Zener mechanical elements (e.g. Carcione *et al*., 2006; Picotti and Carcione, 2017). In acoustic wave simulations, the rock bulk modulus is determined by considering the Brie equation for the fluid mixture; instead, viscoelasticity can be implemented by fitting the Johnson attenuation factors with the Cole-Cole model.

2. Acoustic properties of the fluids

The properties of the fluids involved in the sequestration process (H_2, CO_2, CH_4, and brine) depend on the temperature and pressure, which, in turn, depend on the depth, z. A simple – reference – situation is to consider a constant geothermal gradient, G, so that the temperature variation with depth is:

$$T_c = T_0 + Gz \,, \tag{1}$$

where T_0 is the surface temperature (typical values for G are between 20 and 30 °C/km). The pore pressure, p, at depth z depends on many factors, most of which are geological in nature, e.g. regions of low permeability, sealing faults and hydrocarbon caps that prevent pressure equalisation (communication) from the reservoir to the surface. The simplest case is that the pore pressure is hydrostatic and given by:

$$p = p_0 + \bar{\rho}_b g z \,, \tag{2}$$

where p_0 is the atmospheric pressure, $\bar{\rho}_b$ is the average brine density from the surface to depth z, and g is the acceleration due to gravity. In addition, the confining pressure can be expressed as:

$$p_c = p_0 + \bar{\rho} g z \,, \tag{3}$$

where $\bar{\rho}$ is the average density of the sediments.

2.1. The properties of H_2, CO_2 and CH_4

The thermodynamic properties of real gases can be computed with an EoS. The first cubic EoS was proposed by van der Waals (1873) and is given by:

$$p = \frac{RT_c}{(V-b)} - \frac{a}{V^2}\ , \tag{4}$$

where p is the gas pressure, V is the molar volume, R = 8.31 J/(mol K) is the gas constant, and a and b are the attractive and repulsive terms, respectively, which depend on the chemical compound in question. These coefficients can be calculated as follow (e.g. Poling *et al*., 2001):

$$a = \Omega_a \frac{R^2 T_{cr}^2}{p_{cr}} \tag{5}$$

and

$$b = \Omega_b \frac{RT_{cr}}{p_{cr}}\ , \tag{6}$$

where Ω_a = 0.4218 and Ω_b = 0.125, and T_{cr} and p_{cr} are the critical temperature and pressure, respectively. The critical properties of CO_2, CH_4 and H_2 are listed in Table 1.

Table 1 - Critical properties, molar mass and acentric factor of CO_2, CH_4 and H_2 (from Poling *et al.*, 2001).

Substance	T_{cr} (K)	p_{cr} (MPa)	V_{cr} (cm³/mol)	M (g/mol)	$\bar{\omega}$
CO_2	304.12	7.37	94.07	44.010	0.225
CH_4	190.56	4.56	98.60	16.043	0.011
H_2	33.25	1.30	65.00	2.016	-0.2202

Several EoSs have been published after van der Waals. The PR EoS is a modification of the VDW EoS and is widely used in industrial applications of natural gas. It is given by (Peng and Robinson, 1976):

$$p = \frac{RT_c}{(V-b)} - \frac{a\alpha(T_c)}{V^2+2Vb-b^2}, \tag{7}$$

where the terms a and b are given by Eqs. (5) and (6) with Ω_a = 0.45724 and Ω_b = 0.07780. The temperature dependency of a is provided by the α-function:

$$\alpha(T_c) = \left[1 + m\left(1 - \sqrt{T_r}\right)\right]^2, \tag{8}$$

where $T_r = T_c / T_{cr}$ is the reduced temperature and

$$m = \begin{cases} 0.37464 + 1.54226\bar{\omega} - 0.26992\bar{\omega}^2 & \bar{\omega} \le 0.49 \\ 0.379642 + 1.487503\bar{\omega} + 0.164423\bar{\omega}^2 + 0.016666\bar{\omega}^2 & \bar{\omega} > 0.49 \end{cases} \quad (9)$$

where $\bar{\omega}$ is the acentric factor. The acentric factors of CO_2, CH_4, and H_2 are given in Table 1.

A common strategy to improve the accuracy of PR EoS predictions is to change the α-function specifically for each chemical compound. For CO_2 Hekayati *et al*. (2016) propose the following α-function:

$$\alpha(T_c) = 1.0010 + \ln(p_r)\{0.0524 + 0.2315\ln(T_r) - 0.1286\ln^2(T_r) - 0.3258\sin[0.0704\ \ln^2(p_r)]\} - 0.9461\sin[\ln(T_r)] \quad , \quad (10)$$

where $p_r = p / p_{cr}$ is the reduced pressure. Saffari and Zahedi (2013) developed a new α-function optimised for natural gas components which, for CH_4 is given by

$$\alpha(T_c) = \exp\left[0.039\ T_r\ +\ 0.0473\ln(T_r) +\ 0.8514\left(1\ -\ \sqrt{T_r}\right)\right]. \quad (11)$$

The same parameters are assumed for both CH_4 and H_2.

In the following, we refer to Eq. (7) as the classical Peng-Robinson (CPR) equation with the α-function given by Eq. (8) and the same Eq. (7) as the modified Peng-Robinson (MPR) equation with the α-function given by Eqs. (10) or (11), depending on the type of gas taken into consideration.

The mass density of gases is given by

$$\rho_g = \frac{M}{V}\ , \quad (12)$$

where M is the molar mass and V is the molar volume obtained at given pressure and temperature conditions by solving Eqs. (4) or (7). The molar mass of the gases considered in this study are listed in Table 1. If the gas pressure is assumed to be equal to the expected formation pressure, then ρ_g can be related to depth with Eq. (2).

Isothermal gas compressibility C_T depends on the pressure. It can be calculated as follows (Morse and Ingard, 1986):

$$C_T\ = \frac{1}{\rho_g}\frac{\partial \rho_g}{\partial p}. \quad (13)$$

For sound waves below approximately 1 GHz a better approximation is to assume that the compression is adiabatic, i.e. that the entropy content of the gas remains almost constant during compression (Morse and Ingard, 1986). Adiabatic compressibility C_S is related to isothermal compressibility C_T by $C_S = C_T / \gamma$, where γ is the specific heat ratio.

Considering the VDW EoS [Eq. (4)] and Eq. (12), the gas bulk modulus can be obtained from:

$$K_g = \frac{\gamma}{C_T} = \gamma\left[\frac{VRT_c}{(V-b)^2} - \left(\frac{2a}{V^2}\right)\right]. \quad (14)$$

The specific heat ratio depends on both pressure and temperature (e.g. Schappert and Pelster, 2018), however, $\gamma \approx 7/5$ for H_2 and $\gamma \approx 4/3$ for CH_4 are considered, i.e. the ideal-gas approximations of diatomic and non-linear polyatomic gases, respectively. For CO_2, γ =1.3 is considered (Shearwood and Sloan, 2023).

Considering Eqs. (7) and (12), the gas bulk modulus can be expressed as:

$$K_g = \frac{\gamma}{c_T} = \gamma \left[\frac{VRT_c}{(V-b)^2} - \left(\frac{2a\alpha(V+b)}{V^2+2Vb-b^2} \right)^2 \right]. \quad (15)$$

For this EoS, γ (p, T) is obtained by fitting γ values resulting from velocity data regression. Isothermal series of velocity values from the National Institute of Standards and Technology (NIST) Chemistry WebBook (Linstrom and Mallard, 2001) and densities from the MPR EoS are used to calculate bulk modulus values, which are used as calibration points. Next, the corresponding γ values are calculated using Eq. (15). These sparse data points are, then, fitted using a neural network fitting algorithm (S0852306, 2023), which also enables the estimation of intermediate γ values that are different from those obtained from the calibration points.

Alternative expressions for the acoustic properties of gases can be found in Batzle and Wang (1992), Span and Wagner (1996), and Picotti *et al*. (2012).

The equations providing the viscosities of the three gases as a function of pressure and temperature are reported in Appendix A.

2.2. The properties of brine

The properties of brine depend on the temperature, pressure, and salinity. Batzle and Wang (1992) provide a number of useful empirical relationships between the state variables and the velocity and density. For the sake of completeness, these relationships are reproduced here. The equations are limited to the pressures and temperatures of the experiments conducted by Batzle and Wang (1992) (approximately 60 MPa and 100 °C).

The density of brine, in g/cm^3, is given by:

$$\rho_b = \rho_w + S\{0.668 + 0.44\,S + 10^{-6}[300\ p - 2400\,p\,S + T_c(80 + 3\,T_c - 3300\,S - 13\,p + 47\,p\,S)]\}, \quad (16)$$

with

$$\rho_w = 1 + 10^{-6}(-80\,T_c - 3.3\,T_c^2 + 0.00175\,T_c^3 + 489\,p - 2\,T_c\,p + 0.016\ T_c^2\,p - 1.3 \times 10^{-5}\,T_c^3\,p - 0.333\,p^2 - 0.002\,T_c\ p^2), \quad (17)$$

where S is the weight fraction (ppm/1,000,000) of sodium chloride. Ultimately, the velocity of sound in brine is:

$$V_b = V_w + S\,(1170 - 9.6\,T_c + 0.055\,T_c^2 - 8.5 \times 10^{-5}\,T_c^3 + 2.6\,p - 0.0029\,T_c\,p - 0.0476\,p^2) + S^{1.5}(780 - 10\,p + 0.16\,p^2) - 1820\,S^2, \quad (18)$$

where V_w is the velocity of pure water given by:

$$V_w = \sum_{i=0}^{4} \sum_{j=0}^{3} \omega_{ij} \; T_c^i \; p^j, \tag{19}$$

with constants ω_{ij} given in Table 2. The same units introduced earlier, are used here and in the rest of the paper. Using these relationships, we obtain the brine bulk modulus as $K_b = \rho_b \, V_b^2$.

The viscosity of brine, in mPa s, is computed with:

$$\eta_b = 0.1 + 0.333\, S + (1.65 + 91.9\, S^3) \exp\{-[0.42(S^{0.8} - 0.17)^2 + 0.045]\, T_c^{\,0.8}\}, \tag{20}$$

where T_c is given in degrees Celsius.

Table 2 - Coefficients for brine property calculation.

$\omega_{00} = 1402.85$	$\omega_{20} = 3.437\times10^{-3}$
$\omega_{10} = 4.871$	$\omega_{12} = 1.739\times10^{-4}$
$\omega_{20} = -0.04783$	$\omega_{22} = -2.135\times10^{-6}$
$\omega_{30} = 1.487\times10^{-4}$	$\omega_{32} = -1.455\times10^{-8}$
$\omega_{40} = -2.197\times10^{-7}$	$\omega_{42} = 5.230\times10^{-11}$
$\omega_{01} = 1.524$	$\omega_{03} = -1.197\times10^{-5}$
$\omega_{11} = -0.0111$	$\omega_{13} = -1.628\times10^{-6}$
$\omega_{21} = 2.747\times10^{-4}$	$\omega_{23} = 1.237\times10^{-8}$
$\omega_{31} = -6.503\times10^{-7}$	$\omega_{33} = 1.327\times10^{-10}$
$\omega_{41} = 7.987\times10^{-10}$	$\omega_{43} = -4.614\times10^{-13}$

2.3. The effective fluid model

The mixture of gas and brine behaves like a composite fluid with properties that depend on the stiffness moduli of the constituents and their respective saturations, s_g and s_b, where the indices *g* and *b* refer to gas and brine. The properties of the gas-brine mixture are determined using the Wood model (Wood, 1955; Mavko *et al*., 2009). The bulk modulus is:

$$K_W = \left(s_g K_g^{-1} + s_b K_b^{-1}\right)^{-1}, \tag{21}$$

where $s_b = 1 - s_g$.

If the fluids in the pore volume are not mixed but distributed in patches, the effective bulk modulus of the fluid at high frequencies is larger than that predicted by the Wood model. The differential equations used to calculate synthetic seismograms should take into account the attenuation mechanism of wave-induced fluid flow, also called mesoscopic attenuation. However this approach, which is described for example by the Johnson model, is in the frequency domain. Since modelling in this domain is less efficient, the equations are solved in the time domain, using an effective fluid modulus and viscoelasticity to describe the attenuation (Carcione *et al*., 2006). To obtain the bulk modulus of the gas-liquid mixture, an empirical law, introduced by Brie *et al*. (1995), is applied. The effective bulk modulus is given by:

$$K_B = \left(K_b - K_g\right)s_b^e + K_g\,, \tag{22}$$

where *e* is an empirical parameter. This equation fits the seismic and ultrasonic band data, in particular the values for the sonic band given by Brie *et al*. (1995). Eq. (22) yields the Voigt mixing law (Voigt, 1928) for *e* = 1 and an approximation to the Wood model for *e* = 40. To quantify the exponent, *e*, on a physical basis, in this study, the Johnson model with patchy saturation (Johnson, 2001; Picotti and Carcione, 2017) is used. It is assumed that the medium is provided with gas patches in a brine-saturated background where the brine has absorbed the maximum amount of gas. The Johnson model describes wave velocity and attenuation as a function of frequency, patch size, permeability, and viscosity. Attenuation and velocity dispersion are caused by fluid flow between patches with different pore pressures. The critical relaxation scale of fluid diffusion is proportional to the square root of the ratio of permeability to frequency. At seismic frequencies, the length scale is very large and the pressure is nearly uniform throughout the medium, but as the frequency increases, pore pressure differences can cause a significant increase in P-wave velocity (see Appendix B).

The density of the gas-liquid mixture is simply:

$$\rho_f = s_g\,\rho_g + s_b\,\rho_b. \tag{23}$$

3. Seismic velocities and quality factor

The behaviour of the dry frame (or skeleton) as a function of the confining and pore pressures is an important property of rocks. According to the Krief model, the dry-rock moduli present the following general form (Krief *et al*., 1990):

$$K_m = K_s(1-\phi)^{A/(1-\phi)}, \qquad \mu_m = \frac{B\,\mu_s}{K_s}\,K_m\,, \tag{24}$$

where K_s and μ_s are the bulk and shear moduli of the grains forming the sediment, and *A* and *B* are dimensionless parameters. In order to include the pressure dependence of the dry-rock moduli, the porosity is assumed to be given by (Athy, 1930):

$$\phi = \phi_0 \exp\left(-p_d/p_\phi\right), \tag{25}$$

where ϕ_0 is the porosity at zero differential pressure, for instance, the rock at room conditions, and p_ϕ is a constant.

The rock permeability can be estimated with the Kozeny-Carman equation (Mavko *et al*., 2009):

$$\kappa = \frac{\kappa_0 \phi^3}{(1-\phi)^2}, \tag{26}$$

where κ_0 is a constant.

The wet-rock bulk modulus is given by the Gassmann modulus:

$$K_G(K_f) = K_m + \bar{\alpha}^2 \bar{M}(K_f), \tag{27}$$

where K_f is the bulk modulus of the fluid in the pore space, and

$$\bar{\alpha} = 1 - \frac{K_m}{K_s} \quad \text{and} \quad \bar{M}(K_f) = \left(\frac{\bar{\alpha}-\phi}{K_s} + \frac{\phi}{K_f}\right)^{-1} \tag{28}$$

(e.g. Carcione, 2022). In the case of a gas-brine mixture, K_f can be either K_W or K_B, depending on the distribution of the two fluid phases in the pore space. The wet-rock shear modulus is simply the same as the dry-rock modulus, i.e. $\mu = \mu_m$. The P-wave and S-wave velocities (at low frequencies), therefore, are:

$$V_P = \sqrt{\frac{K_G + 4\mu/3}{\rho}}, \text{ and } V_S = \sqrt{\frac{\mu}{\rho}}, \tag{29}$$

where ρ is the rock bulk density, given by:

$$\rho = (1 - \phi)\rho_s + \phi\rho_f, \tag{30}$$

where ρ_s is the grain density. The Gassmann model provides the velocities when gas and liquid are mixed in the pore space; however, the use of Eq. (22) enables the extension of this model to patchy saturations.

P-wave attenuation and dispersion are introduced with the Johnson patchy saturation model (Johnson, 2001; Picotti and Carcione, 2017). The complex velocity of the P-wave, v_c, is given in Appendix B [Eq. (B13)]. From this velocity, phase velocity v_p, quality factor Q and attenuation factor $\hat{\alpha}$ can be derived as follows (e.g. Carcione, 2022):

$$v_P = \left[\mathrm{Re}\left(\frac{1}{v_c}\right)\right]^{-1}, \tag{31}$$

$$Q = \frac{\mathrm{Re}(v_c^2)}{\mathrm{Im}(v_c^2)} \tag{32}$$

and

$$\hat{\alpha} = -\omega\, \mathrm{Im}\left(\frac{1}{v_c}\right), \tag{33}$$

where $\omega = 2\pi f$ is the angular frequency.

For time-domain numerical modelling and computation of synthetic seismograms, an equivalent viscoelastic medium, represented by the Cole-Cole model (Picotti and Carcione,

2017), is used to account for the attenuation and velocity dispersion described by the Johnson model. The Cole-Cole model is described in Appendix C. The Johnson model has two important parameters that determine the shape and mean size of the patches, namely size factor T and shape factor S/V (see Appendix B). The procedure requires the fitting of the Johnson quality factor [Eq. (32)] to the Cole-Cole quality factor:

$$\tilde{Q} = \frac{\mathrm{Re}(\tilde{v}_c^2)}{\mathrm{Im}(\tilde{v}_c^2)}, \tag{34}$$

associating K [see Eq. (B8)] with $K_G \tilde{M}$ [see Eq. (C1)], where:

$$\tilde{v}_c(\omega) = \sqrt{\frac{K_G \tilde{M}(\omega) + 4\mu/3}{\rho}} \tag{35}$$

is the Cole-Cole complex velocity. In this way, the central frequency, f_C, and the minimum quality factor of the Cole-Cole model, Q_0, are obtained from Q_K = Re (K) / Im (K), and the corresponding parameters (relaxation times and the irrational exponent) are derived from these quantities, as shown in Picotti and Carcione (2017). If ω = 0 and $\tilde{M}$ = 1, then, V_p of Eq. (29) is obtained. Conversely, the S-wave velocity is frequency-independent, since the wave loss is exclusively due to dilatational deformations.

The governing differential equations in 3D space are given by Eq. (15) in Carcione *et al*. (2021):

$$\begin{aligned} \ddot{u}_i &= \rho^{-1}\partial_j \sigma_{ij}, \quad i,j = 1 \dots 3, \\ \sigma + \tau_\sigma^q \frac{\partial^q \sigma}{\partial t^q} &= K_G \left(\varepsilon + \tau_\varepsilon^q \frac{\partial^q \varepsilon}{\partial t^q} \right), \\ \sigma_{ij} &= \mu\, \varepsilon_{ij}, \quad i \neq j, \end{aligned} \tag{36}$$

where u_i represents the displacement components, $\sigma = \sigma_{ii}/3$, $\varepsilon = \varepsilon_{ii}$, an overdot indicates temporal differentiation and Einstein implicit summation is assumed. When q = 1, the Zener model is obtained. The differential equations based on memory variables can be found in section 3.9 of Carcione (2022).

4. Seismic properties of gas bearing rocks

In this study, the density of gases is calculated as a function of depth using the VDW [Eq. (4)] and PR [Eq. (7)] EoSs, while the bulk modulus is calculated using Eqs. (14) and (15). *In-situ* pressure and temperature are determined using Eqs. (1) and (2), where $\bar{\rho}_b$ = 1020 kg/m^3, G = 30 °C/km, and T_0 = 15 °C. Fig. 1a shows the gas densities calculated with different EoSs in comparison with reference data from the NIST Chemistry WebBook. The MPR EoS data match the NIST data points, while the curves calculated with VDW and CPR EoSs deviate from the reference data points. The velocity curves are shown in Fig. 1b, where the velocity of sound in gases is given by:

$$V_g = \sqrt{\frac{K_g}{\rho_g}}. \tag{37}$$

H_2 has a high velocity due to its low density, and CH_4 has a higher velocity than CO_2 due to its lower density. Similarly to Fig. 1a, the MPR EoS performs better than the other equations; therefore, hereafter, the seismic properties of the three gases are calculated with the MPR EoS.

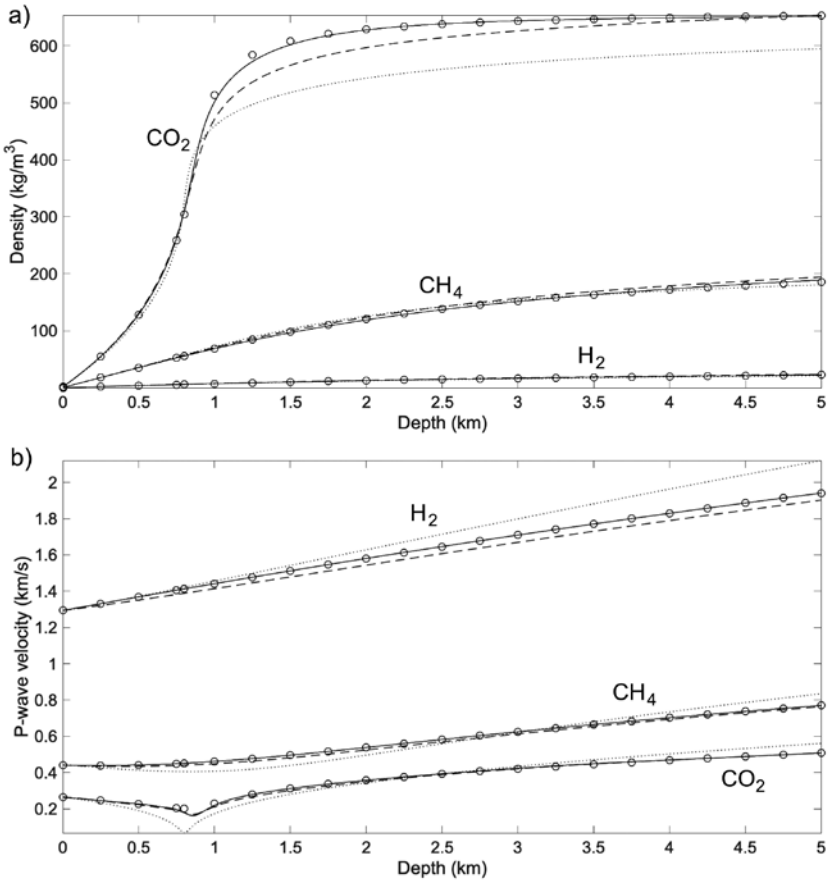

Fig. 1 - Density (a) and sound velocity (b) of CO_2, CH_4 and H_2 as a function of depth; the circles are data obtained from the NIST Chemistry WebBook, the dotted line has been computed with the VDW EoS whilst the dashed and continuous lines have been obtained with the CPR and MPR EoSs, respectively.

As described in section 2.1, the gas bulk modulus depends on the specific heat ratio. Fig. 2 shows γ (p, T_c) of the three gases obtained with Eq. (15) by regressing velocity data from the NIST Chemistry WebBook and fitting it with a neural network algorithm (S0852306, 2023). Such algorithm enables the estimation of the value in the range of 10 - 250 °C and 0 - 50 MPa.

Fig. 3 shows the H_2, CO_2 and CH_4 viscosity values, calculated with the LBC model (Appendix A), compared to values from the NIST Chemistry WebBook; the two data sets slightly differ, yet, in general, are in agreement.

The density and P-wave velocity of brine (S = 50,000 ppm) as a function of depth are shown in Fig. 4. The density decreases with depth, while the P-wave velocity increases down to a depth of 3,000 m and, then, decreases.

Fig. 5 shows the viscosity of brine computed with Eq. (20); its value decreases with depth due to the temperature increasing.

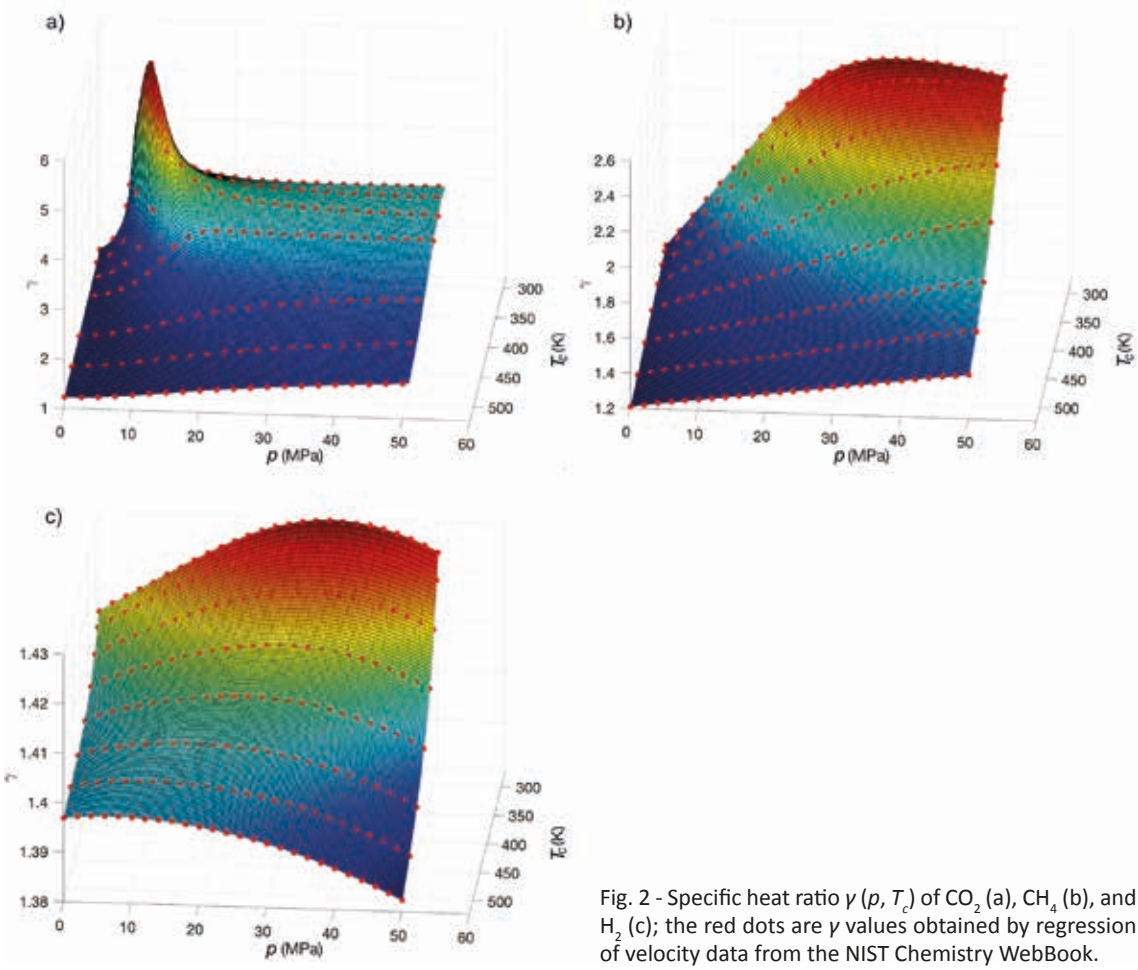

Fig. 2 - Specific heat ratio γ (p, T_c) of CO_2 (a), CH_4 (b), and H_2 (c); the red dots are γ values obtained by regression of velocity data from the NIST Chemistry WebBook.

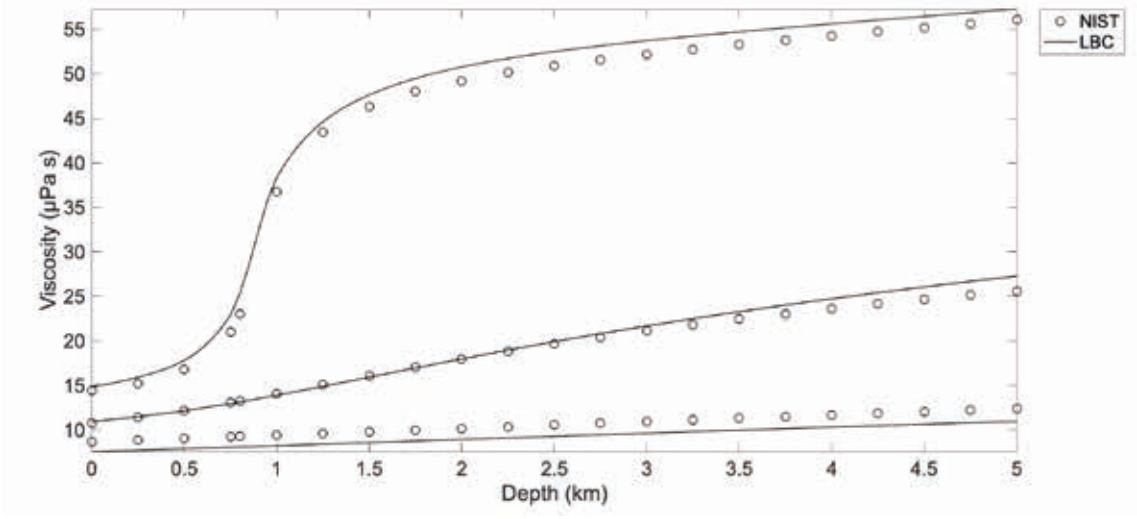

Fig. 3 - Viscosity of CO_2, CH_4 and H_2 as a function of depth computed with the LBC model compared with data from the NIST Chemistry WebBook.

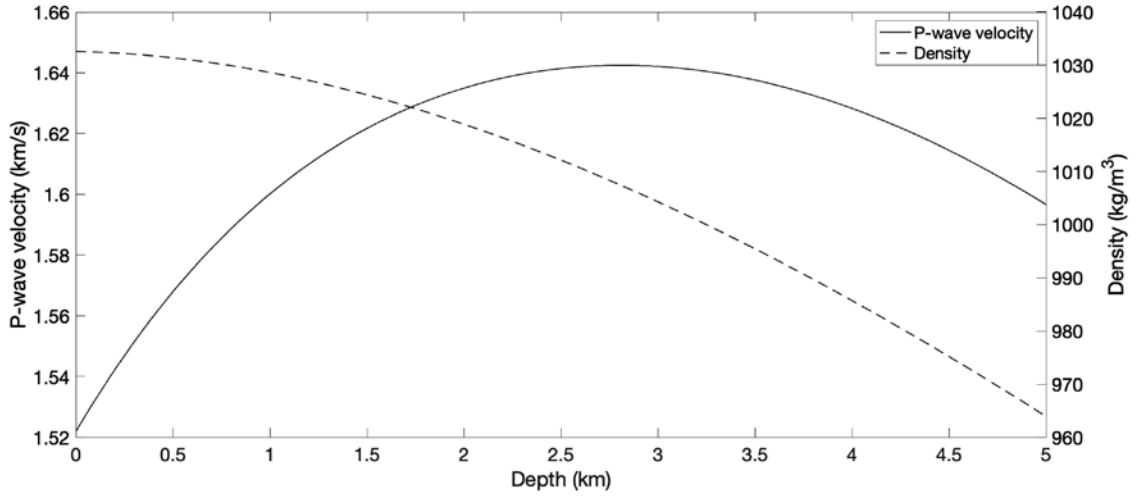

Fig. 4 - Density (dashed curve) and P-wave velocity (continuous curve) of brine as a function of depth.

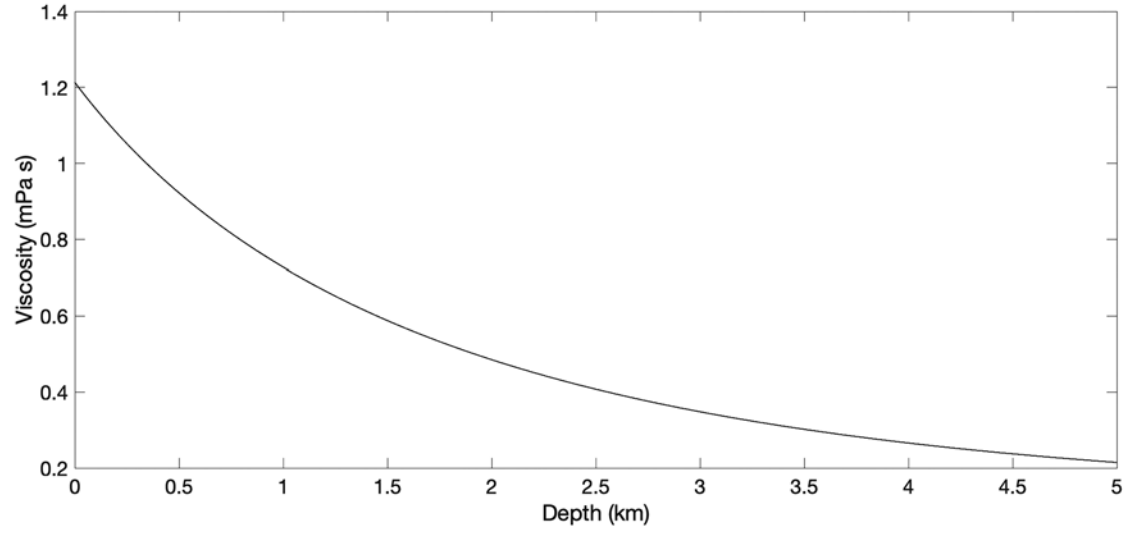

Fig. 5 - Viscosity of brine as function of depth.

To model the seismic properties of gas-bearing rocks, a Utsira-like sand characterising the Sleipner CO_2 reservoir in the central North Sea is considered (e.g. Arts *et al.*, 2004). It is a predominantly sandy unit of late Miocene and early Pliocene age with 30% porosity and a mineralogical composition of quartz (70%), feldspar (10%), mica (5%), calcite (5%), clay (5%), and illite (5%). The average mineral moduli are obtained using the average of the Hashin-Shtrikman bounds (Hashin and Shtrikman, 1963); more precisely, K_s = 40 GPa and μ_s = 38 GPa. The density of the composite solid material is given by:

$$\rho_s = \sum_{i=1}^{N} f_i \, \rho_i \quad , \tag{38}$$

where f_i is the fraction of the *i*-th mineral per unit volume of total solid and ρ_i is its density; ρ_s = 2600 kg/m^3 is obtained. The following properties are also assumed: G = 30 °C/km, $\bar{\rho}_b$ = 1020 kg/m^3, $\bar{\rho}$ = 2300 kg/m^3, ϕ_0 = 0.36, p_ϕ = 50 MPa, A = 6.8, B = 0.63, S = 50,000 ppm, and κ_0 = 8 darcy.

The properties of the sediment and fluids are calculated at depths of 800 and 3,000 m, and are summarised in Table 3. To model the anelastic properties of the rock, the Johnson model with patchy saturation (see Appendix B) and a seismic frequency of f = 30 Hz is used. Two different patch geometries are considered, namely the concentric sphere geometry and a fractal (irregular) geometry. In the first case, an inner gas-saturated sphere is surrounded by an outer brine-saturated sphere with a radius of 30 cm. To obtain the fractal patch, we proceed as described in Picotti *et al*. (2010): the starting point is a spherical patch with size factor T and shape factor S/V, followed by the deformation of the patch from a sphere to a fractal rough shape, by maintaining T constant and multiplying S/V of the original spherical patch by a factor of 10.

Table 3 - Sediment and fluid properties at 800 m and 3,000 m of depth.

	Depth 800 m	**Depth 3,000 m**
Physical conditions	p = 8.1 MPa	p = 30.1 MPa
	p_c = 18.2 Mpa	p_c = 67.8 MPa
	T_c = 39 °C	T_c = 105 °C
Sediment	ϕ = 0.29	ϕ = 0.17
	K_m = 1.39 GPa	K_m = 8.75 GPa
	μ_m = 0.83 GPa	μ_m = 5.23 GPa
	κ = 0.41 darcy	κ = 0.06 darcy
Brine	K_b = 2.6 GPa	K_b = 2.7 GPa
	ρ_b = 1030 kg/m^3	ρ_b = 1004 kg/m^3
	η_b = 0.80 mPa s	η_b = 0.35 mPa s
CO_2	K_g = 9.97 MPa	K_g = 115.71 MPa
	ρ_g = 310 kg/m^3	ρ_g = 644 kg/m^3
	η_g = 25.25 µPa s	η_g = 53.72 µPa s
CH_4	K_g = 11.37 MPa	K_g = 59.17 MPa
	ρ_g = 56 kg/m^3	ρ_g = 152 kg/m^3
	η_g = 13.13 µPa s	η_g = 21.67 µPa s
H2	K_g = 11.98 MPa	K_g = 48.90 MPa
	ρ_g = 6 kg/m3	ρ_g = 17 kg/m3
	η_g = 8.08 µPa s	η_g = 9.62 µPa s

Fig. 6 shows the P-wave velocity as a function of brine saturation for the Utsira-like sand partially saturated with CO_2, CH_4, and H_2 at 800 and 3,000 m of depth. These properties were determined using the Johnson model with spherical patches (solid line) and the Gassmann equation, where the modulus of the pore-fluid mixture is calculated using either the Wood formula [Eq. (21)] (dashed line) or the Brie equation [Eq. (22)] (dotted line). To quantify the Brie exponent, e, the P-wave velocity [Eq. (31)] is fitted as a function of saturation with Eq. (29) using the effective fluid modulus from Eq. (22). At a depth of 800 m, the Brie coefficient is e = 7.3 for the three gases and provides a fairly good fit to the Johnson curves. For z = 3,000 m, the Brie coefficient is e = 5 for H_2 and 4.6 for CO_2 and CH_4.

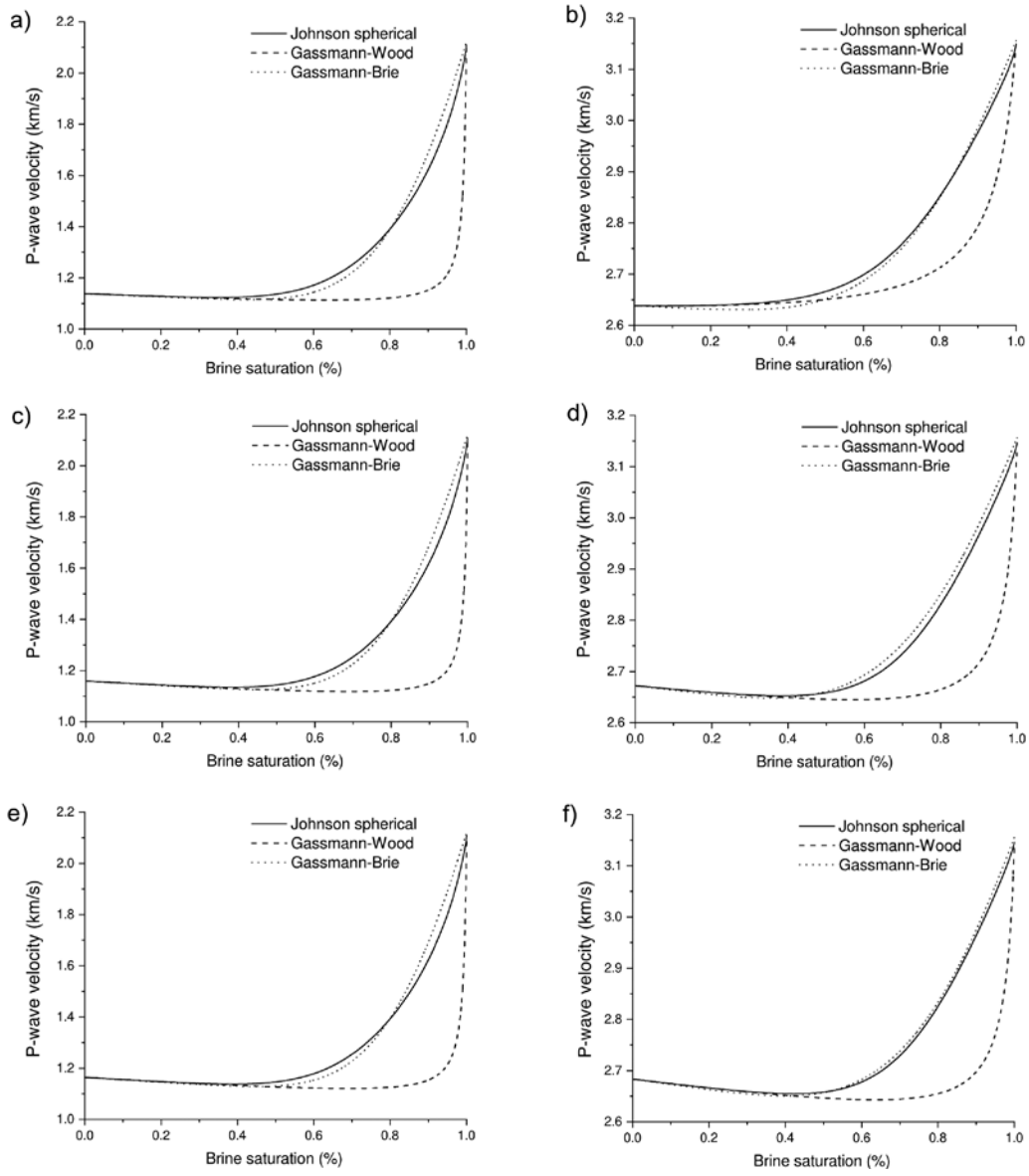

Fig. 6 - Seismic P-wave velocity as a function of brine saturation for CO_2 at 800 m (a) and 3,000 m (b) of depth; CH_4 at 800 m (c) and 3,000 m (d) of depth; and H_2 at 800 m (e) and 3,000 m (f) of depth. The seismic frequency is f = 30 Hz.

The P-wave velocity and dissipation factor (1,000/Q) determined with the Johnson model for spherical and fractal gas patches, as a function of brine saturation and at depths of 800 and 3,000 m, are shown in Fig. 7. At shallower depths, the velocity and attenuation of the partially saturated sediment are very similar, regardless of the gas and saturation value considered. In contrast, these seismic properties differ at 3000 m of depth, especially for CO_2 compared to CH_4 and H_2.

Fig. 8 shows the P-wave velocity and the dissipation factor of the Utsira-like sand partially saturated with the three gases (s_b = 0.8) as a function of frequency at z = 800 m (Figs. 8a and 8b) and z = 3,000 m (Figs. 8c and 8d). The attenuation, due to mesoscopic-loss effect, is significant due to the properties of the Utsira-like sand, i.e. high porosity, high permeability, and low frame moduli. As expected, the rock becomes stiffer and less attenuating at 3,000 m of depth.

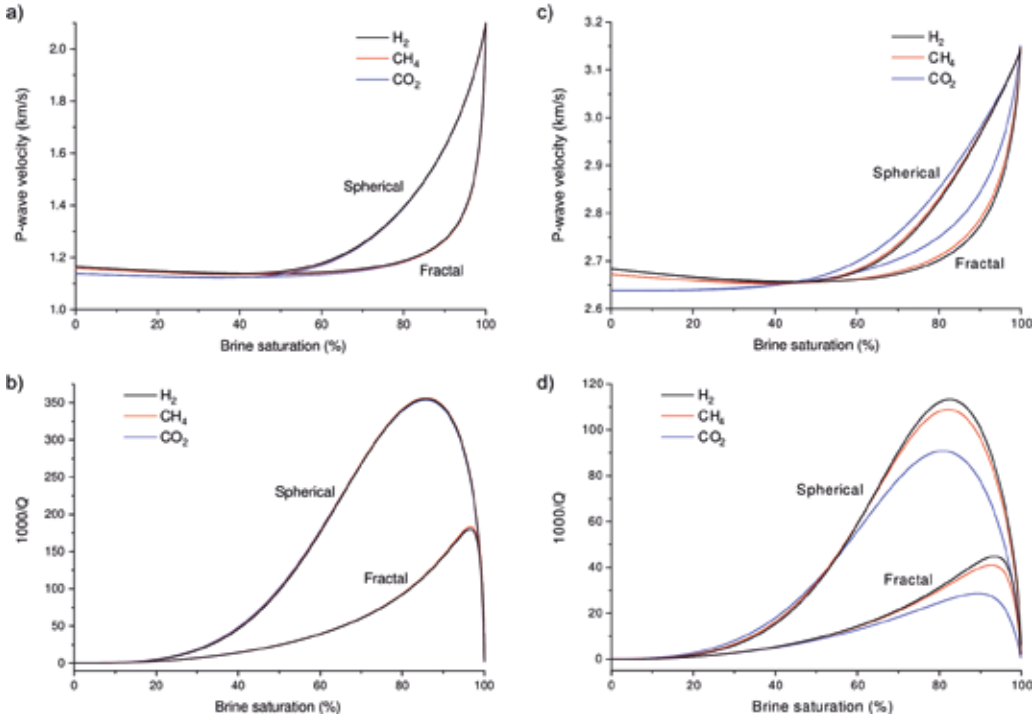

Fig. 7 - The Johnson seismic P-wave velocity and dissipation factor as a function of brine saturation, at 800 m of depth (panels a and b) and 3,000 m of depth (panels c and d). The seismic frequency is f = 30 Hz.

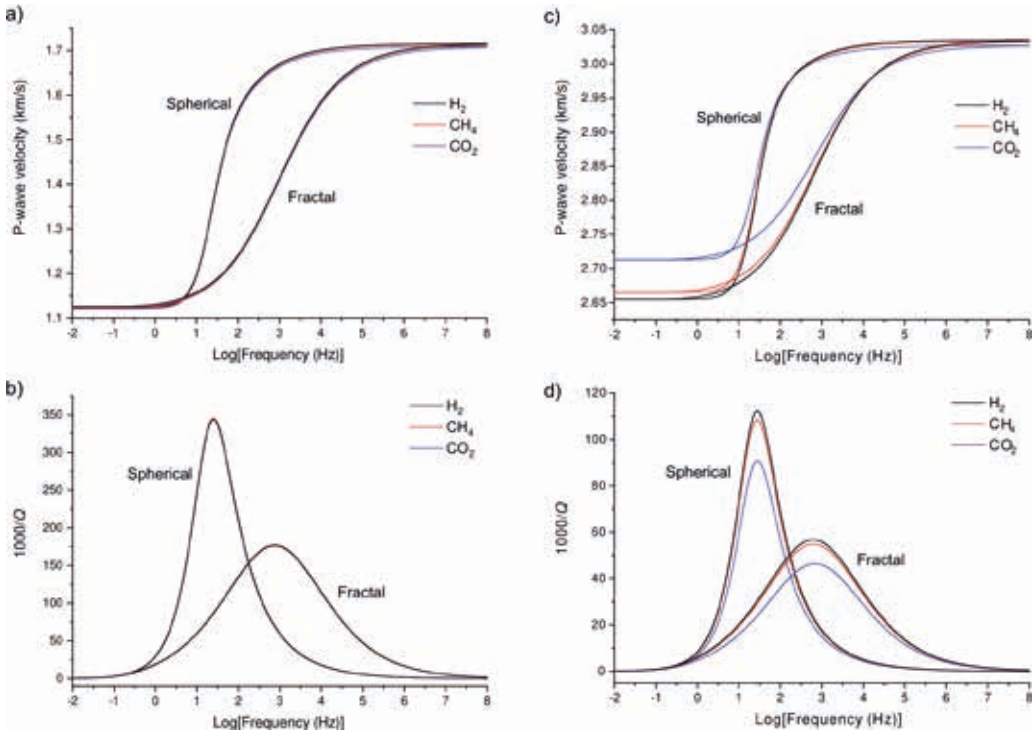

Fig. 8 - The Johnson seismic P-wave velocity and dissipation factor as a function of frequency of a sediment partially saturated (s_b = 0.8) with CO_2, CH_4, and H_2 at 800 m (panels a and b) and 3,000 m of depth (panels c and d).

As observed by Picotti and Carcione (2017) and Picotti *et al*. (2010), the shape of the curves corresponding to the two patch geometries results to be similar, but as the patch irregularity increases, the relaxation peak shifts to higher frequencies while the maximum loss decreases.

Fig. 9 shows the S-wave velocity and density of the Utsira-like sand partially saturated with CO_2, CH_4, and H_2 at 800 m (Fig. 9a) and 3,000 m (Fig. 9b) of depth. The variation in S-wave velocity is due to a density effect, as the wet-rock shear modulus is equal to the dry-rock shear modulus.

An equivalent viscoelastic medium, based on the Cole-Cole model, is taken into consideration for setting up the differential equations for the computation of the synthetic seismograms. Fig. 10 shows the fit of the Johnson P-wave velocity and the dissipation factor as a function of frequency for z = 800 m (Figs. 10a and 10b) and z = 3,000 m (Figs. 10c and 10d). The fits are very

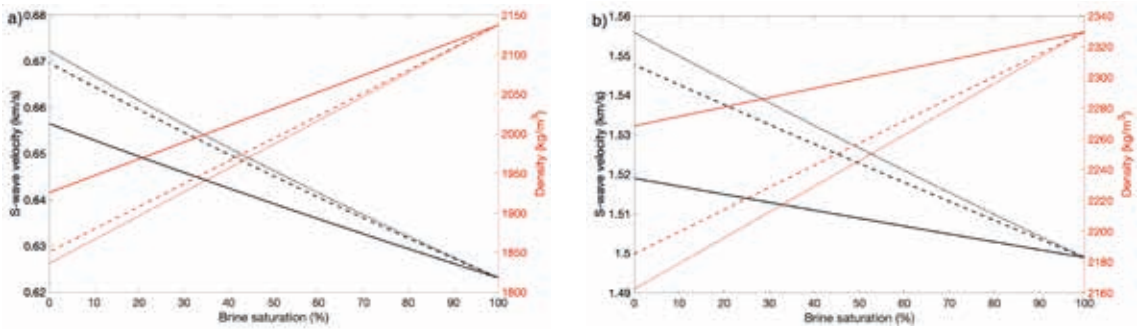

Fig. 9 - Seismic S-wave velocity (black) and density (red) as a function of brine saturation, corresponding to CO_2 (solid lines), CH_4 (dashed lines) and H_2 (dotted lines) for z = 800 m (a) and z = 3,000 m (b).

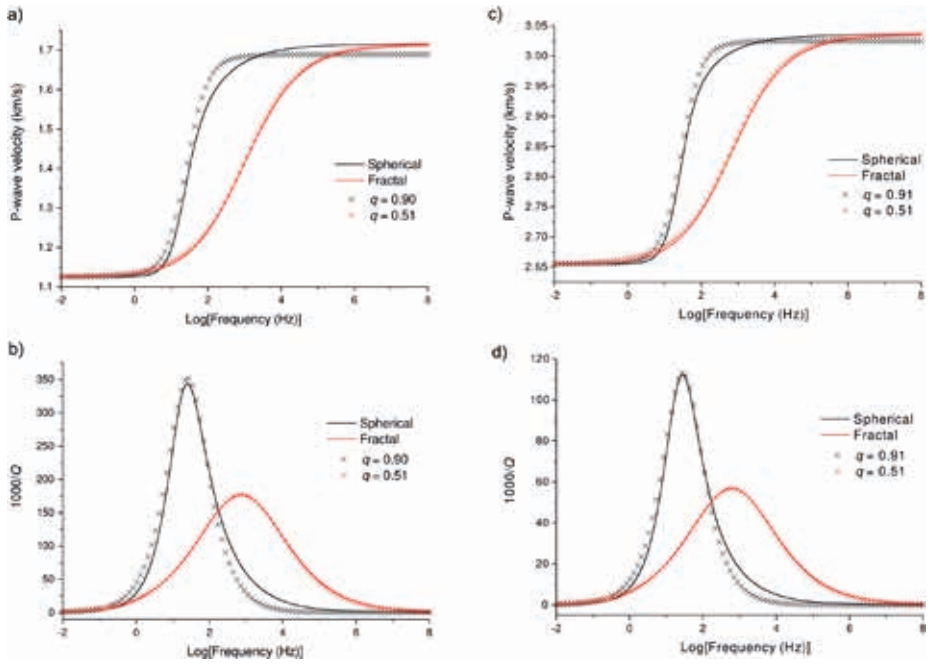

Fig. 10 - Seismic P-wave velocity and dissipation factor as a function of frequency of a sediment partially saturated (s_b = 0.8) with H_2 (solid line) at 800 m (panels a and b) and 3,000 m of depth (panels c and d) and corresponding fits with the Cole-Cole model (crosses).

good, especially in the region of the relaxation peak. Even if the fits at high frequencies are not mathematically perfect, these results show that the Cole-Cole model is a good approximation for practical purposes.

Finally, Fig. 11 shows the attenuation factor as a function of frequency. Within the seismic frequency band, the attenuation is larger at 800 m than at 3,000 m, regardless of the geometry of the gas patches. At sonic frequencies, or higher, the signal is strongly attenuated at 800 m for both the spherical and fractal patch distribution and at 3,000 m for the fractal geometry.

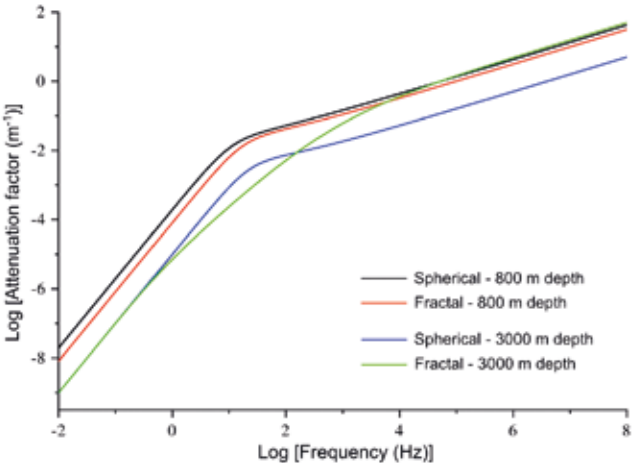

Fig. 11 - Attenuation factor as a function of frequency for a sediment partially saturated with H_2 (s_b = 0.8) at 800 m and 3,000 m of depth and for spherical and fractal patches.

5. Conclusions

The seismic time-lapse method is essential for detecting and monitoring the presence of gas in geological formations. The success of seismic monitoring depends on a correct description of the physical properties of the gas-bearing rock.

In the case of patchy gas saturation, the petro-elastic model predicts higher velocities than in the case where gas and brine are mixed in the pore space. In this study the Brie equation is used to determine the bulk modulus of the gas-brine mixture. Moreover, the Cole-Cole model is used to approximate the seismic velocity and quality factor determined by the mesoscopic Johnson model to compute synthetic seismograms in the time domain. The attenuation due to mesoscopic loss presents a maximum at low gas saturation between 10% and 30% and is significant for the case presented in this work, i.e. for a sandstone with high porosity, high permeability and low framework moduli.

The proposed petro-elastic model enables to directly control reservoir properties such as dry-rock modulus, porosity, permeability, and fluid properties, as well as *in-situ* conditions such as pore pressure and temperature.

REFERENCES

Arts R., Eiken O., Chadwick R.A., Zweigel P., Van der Meer L. and Zinszner B.; 2004: *Monitoring of CO_2 injected at Sleipner using time-lapse seismic data*. Energy, 29, 1383–1392, doi: 10.1016/j.energy.2004.03.072.

Athy L.F.; 1930: *Density porosity, and compaction of sedimentary rocks*. Bull. Am. Ass. Petroleum Geologists, 14, 1–24, doi: 10.1016/j.energy.2004.03.072.

Barison E., Donda F., Merson B., Le Gallo Y. and Réveillère A.; 2023: *An insight into underground hydrogen storage in Italy*. Sustainability, 15, 6886, 21 pp., doi: 10.3390/su15086886.

Batzle M. and Wang Z.; 1992: *Seismic properties of pore fluids*. Geophysics, 57, 1396–1408, doi: 10.1190/1.1443207.

Brie A., Pampuri F., Marsala A.F. and Meazza O.; 1995: *Shear sonic interpretation in gas-bearing sands*. In: SPE Annual Technical Conference, Dallas, TX, USA, Paper no. 30595, pp. 701–710, doi: 10.2118/30595-MS.

Carcione J.M.; 2022: *Wave fields in real media: wave propagation in anisotropic, anelastic and porous and electromagnetic media*. *Fourth edition*. Elsevier, Amsterdam, The Netherlands, 796 pp.

Carcione J.M. and Picotti S.; 2006: *P wave seismic attenuation by slow-wave diffusion: effects of inhomogeneous rock properties*. Geophysics, 71, 1–8, doi: 10.1190/1.2194512.

Carcione J.M., Picotti S., Gei D. and Rossi G.; 2006: *Physics and seismic modeling for monitoring CO_2 storage*. Pure and Applied Geophysics, 163, 175–207, doi: 10.1007/s00024-005-0002-1.

Carcione J.M., Gei D., Picotti S., Misnan M.S., Rashidi M.R.A., Abu Bakar Z.A., Harith Z.Z.T., Samsol Bahri N.M. and Hashim N.; 2020: *Porosity and permeability of the overburden from wireline logs: a case study from offshore Malaysia*. Geomech. Geophys. Geo-energ. Geo-resour., 6, article no. 48, 12 pp., doi: 10.1007/s40948-020-00172-y.

Carcione J.M., Picotti S. and Ba J.; 2021: *P- and S-wave simulation using a Cole-Cole model to incorporate thermoelastic attenuation and dispersion*. J. Acous. Soc. Am., 149, 1946-1954, doi: 10.1121/10.0003749.

Carcione J.M., Gei D. and Picotti S.; 2023: *Acoustics of stored-hydrogen seismic detection in saline aquifers*. In: 5th SEG Rock Physics and Geofluid Detection Workshop, December 8-10, Nanjing, China, extended abstract, https://dxy.hhu.edu.cn/en/2023/1219/c10164a269718/page.htm.

Chabab S., Thveneau P., Coquelet C., Corvisier J. and Paricaud P.; 2020: *Measurements and predictive models of high-pressure H_2 solubility in brine (H_2O+NaCl) for underground hydrogen storage application*. Int. J. Hydrogen Energy, 45, 32206–32220, doi: 10.1016/j.ijhydene.2020.08.192.

Cole K.S. and Cole R.H.; 1941: *Dispersion and absorption in dielectrics. I. Alternating current characteristics*. J. Chem. Phys., 9, 341–351, doi: 10.1063/1.1750906.

Hashin Z. and Shtrikman S.; 1963: *A variational approach to the theory of the elastic behaviour of multiphase materials*. J. Mech. Phys. Solids, 11, 127–140, doi: 10.1016/0022-5096(63)90060-7.

Hekayati J., Roosta A. and Javanmardi J.; 2016: *Volumetric properties of supercritical carbon dioxide from volume-translated and modified Peng-Robinson equations of state*. Korean Journal of Chemical Engineering, 33, 3231–3244, doi: 10.1007/s11814-016-0176-5.

Hill R.; 1964: *Theory of mechanical properties of fiber-strengthened materials*. J. Mech. Phys. Solids, 12, 199–212, doi: 10.1016/0022-5096(64)90019-5.

Johnson D.L.; 2001: *Theory of frequency dependent acoustics in patchy saturated porous media*. J. Acoust. Soc. Am., 110, 682–694, doi: 10.1121/1.1381021.

Krief M., Garat J., Stellingwerff J. and Ventre J.; 1990: *A petrophysical interpretation using the velocities of P and S waves (full waveform sonic)*. The log Analyst, 31, 355–369.

Linstrom P.J. and Mallard W.G.; 2001: *The NIST Chemistry Webbook: A chemical data resource on the internet*. Journal of Chemical & Engineering Data, 46, 1059–1063, doi: 10.1021/je000236i.

Lohrenz J., Bray B.G. and Clark C.R.; 1964: *Calculating viscosities of reservoir fluids from their compositions*. J. Pet. Technol., 16, 1171–1176, doi: 10.2118/915-PA.

Mattera S., Donda F., Tinivella U., Barison E., Le Gallo Y. and Vincent C.; 2023: *First assessment of an area potentially suitable for underground hydrogen storage in Italy*. International Journal of Hydrogen Energy, 48, 17940-17956, doi: 10.1016/j.ijhydene.2023.01.192.

Mavko G., Mukerji T. and Dvorkin J.; 2009: *The rock physics handbook*. *2nd ed*. Cambridge Univ. Press, Cambridge, UK, 511 pp., doi: 10.1017/CBO9780511626753.

Miocic J., Heinemann N., Edlmann K., Scafidi J., Molaei F. and Alcalde J.; 2023: *Underground hydrogen storage: a review*. Geological Society, Special Publications, 528, 73-86, doi: 10.1144/SP528-2022-88.

Morse P.M. and Ingard K.U.;1986: *Theoretical acoustics*. Princeton University Press, Princeton, NJ, USA, 949 pp.

Peng D.Y. and Robinson, D.B.; 1976: *A new two-constant equation of state*. Industrial & Engineering Chemistry Fundamentals, 15, 59–64, doi: 10.1021/i160057a011.

Picotti S. and Carcione J.M.: 2017: *Numerical simulation of wave-induced fluid flow seismic attenuation based on the Cole-Cole model*. J. Acoust. Soc. Am., 142, 134–145, doi: 10.1121/1.4990965.

Picotti S., Carcione J.M., Rubino G., Santos J.E. and Cavallini F.; 2010: *A viscoelastic representation of wave attenuation in porous media*. Comput. Geosci., 36, 44–53, doi: 10.1016/j.cageo.2009.07.003.

Picotti S., Carcione J.M., Gei D., Rossi G. and Santos J.E.; 2012: *Seismic modeling to monitor CO_2 geological storage - The Atzbach-Schwanenstadt gas field*. JGR Solid Earth, 117, 6, B06103, 18 pp., doi:10.1029/2011JB008540.

Poling B.E., Prausnitz J.M. and O'Connell J.P.; 2001: *The properties of gases and liquids*. McGraw Hill, New York, NJ, USA, 768 pp.

S0852306; 2023: *Surface fitting using neural networks*. MATLAB Central File Exchange, <https://www.mathworks.com/matlabcentral/fileexchange/129589-surface-fitting-using-neural-networks>, retrieved 14 December 2023.

Saffari H. and Zahedi A.; 2013: *A new alpha-function for the Peng-Robinson equation of state: application to natural gas*. Chinese Journal of Chemical Engineering, 21, 1155–1161, doi: 10.1016/S1004-9541(13)60581-9.

Schappert K. and Pelster R.; 2018: *Requirements to determine the average pore size of nanoporous media using ultrasound*. ACS Omega, 3, 18906–18910, doi: 10.1021/acsomega.8b03091.

Shearwood C. and Sloan P.A.; 2023: *The Rüchardt experiment revisited: using simple theory, accurate measurement and python based data analysis*. European Journal of Physics, 44, 3, 035102, 26 pp, doi: 10.1088/1361-6404/acc5c2.

Span R. and Wagner W.; 1996: *A new equation of state for carbon dioxide covering the fluid region from the triple-point temperature to 100 K at pressures up to 800 MPa*. Phys. Chem. Ref. Data, 25, 1509–1596, doi: 10.1063/1.555991.

van der Waals J.D.; 1873: *Over de Continuited van den Gasen Vloeistoftoestand*. Doctoral Thesis, University of Leiden, A.W. Sijthoff, Leiden, Germany, 135 pp., <https://www.lorentz.leidenuniv.nl/history/nobel_theses/sources/vanderWaals_1873.pdf>.

Voigt W.; 1928: *Lehrbuch der Kristallphysik (mit Ausschluss der Kristalloptik)*. Taubner, Leipzig, Germany, 978 pp, doi: 10.1007/978-3-663-15884-4.

Wood A.W.; 1955: *A textbook of sound*. MacMillan, New York, NY, USA, 656 pp.

Corresponding author: Davide Gei
Istituto Nazionale di Oceanografia e di Geofisica Sperimentale - OGS
Borgo Grotta Gigante 42/c, 34010 Sgonico (TS), Italy
Phone: +39 040 2140321; e-mail: dgei@ogs.it

Appendix A: the viscosity of gases

The viscosity of gases, η_g, can be computed as a function of the gas density, ρ_g, with the LBC model (Lohrenz *et al*., 1964):

$$\left[(\eta_g - \eta_0)\xi + 10^{-4}\right]^{-0.25} = \sum_{j=0}^{4} a_i \left(\frac{\rho_g}{\rho_{cr}}\right)^j, \tag{A1}$$

where a_0 = 0.10230, a_1 = 0.023364, a_2 =0.058533, a_3 = -0.040758, a_4 = 0.0093324, and $\rho_{cr} = \frac{M}{V_{cr}}$ is the critical density. Critical volumes V_{cr} of H_2, CO_2, and CH_4 are listed in Table 1. The viscosity- reducing parameter is given by:

$$\xi = T_{cr}^{1/6} M^{-1/2} p_{cr}^{-2/3} \tag{A2}$$

and the low-pressure viscosity by:

$$\eta_0 = \begin{cases} 34 \cdot 10^{-5} \dfrac{T_r^{0.94}}{\xi} & T_r \leq 1.5, \\ 17.78 \cdot 10^{-5} \dfrac{(4.58\, T_r - 1.67)^{5/8}}{\xi} & T_r > 1.5. \end{cases} \tag{A3}$$

Appendix B: the Johnson model

A seismic compressional wave travelling through a rock characterised by patchy saturation induces a pressure disequilibrium between brine and gas saturated regions, which tend to equilibrate by developing the diffusive Biot acoustic slow wave. This phenomenon causes wave-velocity dispersion and compressional wave attenuation and is governed by the size and distribution of the patches, frequency, permeability, and porosity of the medium (Johnson, 2001). The wave-induced fluid flow process related to the Biot slow wave is characterised by the critical fluid diffusion relaxation length, given by:

$$L_c = \sqrt{D/\omega}, \tag{B1}$$

where $\omega = 2\pi f$ is the angular frequency and D (K_f) is the diffusivity constant, defined in each saturated region as:

$$D = \frac{\kappa K_E}{\eta}, \tag{B2}$$

where κ is the rock permeability, η is the fluid phase viscosity and K_E is (Carcione and Picotti, 2006):

$$K_E = \frac{E_m \bar{M}}{E_G}. \tag{B3}$$

In this expression, $\bar{M}$ is given by Eq. (28).

$$E_m = K_m + \frac{4}{3}\mu_m \tag{B4}$$

is the dry-rock P-wave modulus, and

$$E_G = K_G + \tfrac{4}{3}\mu_m, \tag{B5}$$

(Carcione, 2022), where K_G (K_f) is the Gassmann bulk modulus [Eq. (27)].

At low frequencies, the patch size is smaller than diffusion length L_c and there is sufficient time for the pore pressure to equilibrate, inducing an isostress regime. In such a case, the effective bulk modulus of the composite medium, at the low frequency limit, is independent of the spatial distribution of the fluids and is given by the Gassmann expression $K_{GW} = K_G(K_W)$, where the effective modulus of the composite pore fluid is given by the Wood equation [Eq. (21)]. In the high-frequency limit, the patch size is larger than L_c and there is no time for pressure equilibration. The pore pressure is not uniform throughout the medium, however, it can be considered constant within each fluid phase. In such a case, the effective bulk modulus is given by the equation (Hill, 1964):

$$K_{GH} = \left(\frac{S_g}{K_G(K_g) + \frac{4}{3}\mu_m} + \frac{S_b}{K_G(K_b) + \frac{4}{3}\mu_m} \right)^{-1} - \frac{4}{3}\mu_m, \tag{B6}$$

where s_g and s_b are the gas and brine saturations, respectively. The high-frequency P-wave modulus is given by

$$E_\infty = K_{GH} + \frac{4}{3}\mu_m. \tag{B7}$$

At intermediate frequencies, the size of the patches and the diffusion length are comparable. In such a case, Johnson (2001) introduced a dynamic bulk modulus:

$$K(\omega) = K_{GH} - \frac{K_{GH} - K_{GW}}{1 - \zeta + \zeta\sqrt{1 - i\omega\tau/\zeta^2}}\ , \tag{B8}$$

where i is the imaginary unit, ζ is a shape parameter and τ sets the frequency scale. When $\zeta < 1$ the crossover region is quite broad, whereas when $\zeta > 1$ it is quite narrow. ζ and τ can be separately computed from parameters S/V and T, which depend on the geometry of the patches (Johnson, 2001; Picotti *et al*., 2010). The specific surface area, S/V, (the ratio between the boundary area separating the two phases, S, and the patch volume, V), is governed by the shape of the patches and, therefore, it is called 'shape factor'. Considering concentric spherical geometries (Johnson, 2001), where an inner gas-saturated sphere of radius a is surrounded by an outer brine-saturated sphere of radius b ($b > a$):

$$S/V = 3\frac{a^2}{b^3}. \tag{B9}$$

The parameter T is governed by the mean size of the patch in a complicated and non-local way, which can be solved only with certain simplifying geometries (Johnson, 2001). For the concentric spherical geometry:

$$\begin{aligned} T = \frac{K_{GW}\phi^2}{30\kappa b^3}\{&[3\eta_2 g_2^2 + 5(\eta_1 - \eta_2)g_1 g_2 - 3\eta_1 g_1^2]a^5 - 15\eta_2\, g_2(g_2 - g_1)a^3 b^2 \\ &+ 5g_2[3\eta_2\, g_2 - (2\eta_1 - \eta_2)g_1]a^2 b^3 - 3\eta_2\, g_2^2\, b^5\}, \end{aligned} \tag{B10}$$

where

$$g_j = \frac{\left(1 - \frac{K_m}{K_s}\right)\left(\frac{1}{K_W} - \frac{1}{K_j}\right)}{1 - \frac{K_m}{K_s} - \phi\frac{K_m}{K_s} + \phi\frac{K_m}{K_W}}, \qquad j = 1,2. \tag{B11}$$

In Eqs. (B10) and (B11) subscripts 1 and 2 indicate the gas and liquid phases, respectively.

Ultimately, the P-wave modulus is:

$$E(\omega) = K(\omega) + \frac{4}{3}\mu_m \tag{B12}$$

and the complex P-wave velocity is:

$$v_c = \sqrt{\frac{K(\omega) + 4\mu_m/3}{\rho}}\ , \tag{B13}$$

where ρ is the rock bulk density [Eq. (30)].

Appendix C: the Cole-Cole model

To obtain the equivalent viscoelastic medium, the Cole-Cole model (Cole and Cole, 1941) is used. The stress-strain relationship in the frequency domain (based on irrational powers of frequency) can be represented in the time domain as a differential equation with fractional order derivatives (e.g. Carcione *et al*., 2021). The dimensionless complex modulus of a Cole-Cole element can be expressed:

$$\tilde{M}(\omega) = \frac{1 + (i\omega\tau_\varepsilon)^q}{1 + (i\omega\tau_\sigma)^q}\,, \tag{C1}$$

where τ_σ and τ_ε are relaxation times, $0 \le q < 2$ is a real number, $i = \sqrt{-1}$ is the imaginary number and $\omega = 2\pi f$ is the angular frequency; $q = 0$ corresponds to the lossless case, while with $q = 1$, the Zener model is obtained (Carcione, 2022). The quality factor related to $\tilde{M}$ is $\mathrm{Re}(\tilde{M})/\mathrm{Im}(\tilde{M})$ where Re and Im denote real and imaginary parts, respectively. The maximum dissipation factor, corresponding to the minimum quality factor is located at:

$$\omega_0 = \frac{1}{\sqrt{\tau_\sigma\,\tau_\varepsilon}} \tag{C2}$$

and is equal to:

$$Q_0 = \frac{(1+\beta^2)\cot\varphi + 2\beta\csc\varphi}{\beta^2 - 1}, \quad \beta = \left(\frac{\tau_\varepsilon}{\tau_\sigma}\right)^{q/2}, \quad \varphi = \frac{\pi q}{2}. \tag{C3}$$

Using ω_0 and Q_0 as parameters, the following is obtained:

$$\tau_\varepsilon = \frac{\beta^{1/q}}{\omega_0}, \qquad \tau_\sigma = \frac{\beta^{-1/q}}{\omega_0}, \tag{C4}$$

where β is a solution of Eq. (C3):

$$\beta = \frac{1 + \sqrt{1+Q_0^2}\,\sin\varphi}{Q_0\,\sin\varphi - \cos\varphi}. \tag{C5}$$

The unrelaxed (high-frequency) modulus is $(\tau_\varepsilon/\tau_\sigma)^q$.

The Cole-Cole model stress (σ)-strain (ε) differential equation, corresponding to the kernel [Eq. (C1)], is (Picotti and Carcione, 2017):

$$\sigma + \tau_\sigma^q \frac{\partial^q \sigma}{\partial t^q} = M_R \left(\varepsilon + \tau_\varepsilon^q \frac{\partial^q \varepsilon}{\partial t^q}\right), \tag{C6}$$

where M_R is a relaxed (low-frequency) stiffness, i.e. the Gassmann modulus.

When $\tau_\varepsilon = 0$, the Kelvin-Voigt model is obtained. If $Q_0 \to \infty$, the low-frequency elastic limit is reached, with $\beta = 1$, $\tau_\varepsilon = \tau_\sigma$ and $\tilde{M} = 1$.